Cylindrical Droplet on Nanofibers: A Step toward the Clam-Shell Drop Description

Gersh O. Berim and Eli Ruckenstein*

Department of Chemical and Biological Engineering, State University of New York at Buffalo, Buffalo, New York 14260

Received: January 3, 2005; In Final Form: April 19, 2005

The existence and shape of a cylindrical (infinitely long) liquid drop on a fiber of arbitrary radius are examined using a microscopic approach based on the interaction potentials between the molecules of the system. A differential equation for the drop profile was derived by the variational minimization of the total potential energy by taking into account the structuring of the liquid near the fiber. This equation was solved by quadrature, and the existence conditions and the shape of the drop were examined as functions of the radius of the fiber, microscopic contact angle θ_0, which the actual drop profile makes with the fiber, and a certain parameter, a, which depends on the interaction potential parameters. Angle θ_0 is defined in the nanoscale range near the leading edge where the interactions between the liquid and solid are strong. It differs from the macroscopically measured wetting angle (θ_m) that represents the extrapolation of the profile outside the range of liquid−solid interaction to the solid surface. Expressions for both θ_0 and θ_m are established in the paper. For any given fiber radius, the range of drop existence involves two domains in the plane $\theta_0 - a$, separated by a critical curve $a = a_c(\theta_0)$. In the first domain, below the curve $a = a_c(\theta_0)$, the drop always exists and can have any height, h_m. In the second domain, above the curve $a = a_c(\theta_0)$, there is an upper limit of h, h_{m1}, such that drops with $h_m > h_{m1}$ cannot exist. The shape of the drop depends on whether the point (θ_0, a) on the $\theta_0 - a$ plane is far from the critical curve or near to it. In the first case, the drop profile has generally a circular shape, with the center of the circle not located on the fiber axis, whereas in the second case the shape is "quasi planar", that is, most of the drop profile lies on a circle concentric with the fiber profile. Comparing the potential energies of a cylindrical drop on a fiber and a film of uniform thickness covering the fiber and having the same volume as the drop, the energetically preferred configuration was determined for various conditions. Considering the cylindrical drop as a limiting case of a clam-shell one, and the film as a limiting case of a barrel drop, the obtained analytical results could be employed to examine the barrel-drop−clam-shell-drop transformation (roll-up transition).

I. Introduction

A liquid droplet placed on a cylindrical surface of a solid (fiber) and immersed in a vapor (gas) can acquire either an axisymmetrical (barrel) or a nonaxisymmetrical (clam-shell) configuration (Figure 1). Experiment[1] showed that the configuration that a given drop takes depends on the drop volume and the conventionally macroscpically determined contact angle between the drop and the fiber. For larger volumes and smaller contact angles, the drop tends to acquire a barrel-like shape. With decreasing volume, that axisymmetrical configuration is transformed through the so-called roll-up transition[2] to a clam-shell configuration. Full theoretical consideration of that transition requires a comparison of the free energies of the two configurations for the same drop volume. An equation for the barrel drop surface was established in numerous papers on the basis of a macroscopic approach[3−7] that involved such quantities as the surface tensions and the disjoining pressure, as well as on the basis of microscopic theories[8,9] based on liquid−liquid and liquid−solid interaction potentials. The obtained solutions provided equations of the surface in explicit form through elliptic integrals[3] or quadratures[7−9] and allowed one to calculate the energy of any given barrel droplet. Carroll[1] has employed his solution for the barrel-drop profile[3] for an indirect theoretical treatment of the roll-up transition by analyzing the stability to small perturbations of its shape. If the profile is not stable, the barrel drop is in a metastable state and can acquire a clam-shell shape. The conditions for existence of a barrel drop were also obtained in ref 8 using a microscopic theory.

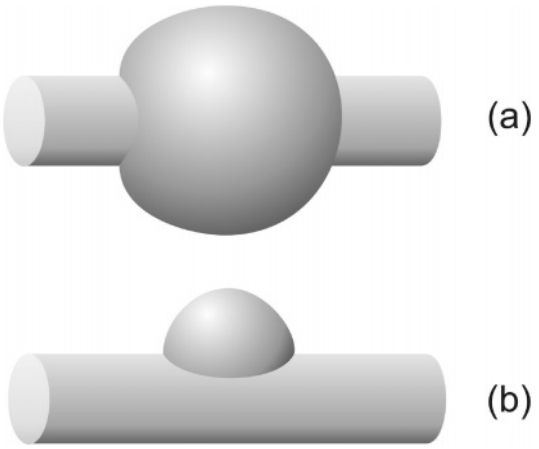

Figure 1. Axisymmetric (a) and clam-shell (b) configurations of a liquid drop on a fiber.

Much less is known about the shape of the clam-shell droplet, for which no analytical results could be obtained because of the complexity of the problem. The only known calculations

* To whom correspondence should be addressed. E-mail: feaeliru@acsu.buffalo.edu; Phone: (716)645−2911, ext. 2214; Fax: (716)645−3822.

10.1021/jp050021l CCC: $30.25
Published on Web 05/25/2005

were carried out by the finite element method[10,11] based on the classical idea of the constancy of the Laplace excess pressure along the drop surface. The necessity of a large-scale computation makes that method inconvinient and any analytical solution highly desirable.

In this paper, the characteristics of a clam-shell droplet profile in a plane that includes the drop apex and is normal to the fiber axis are examined. The profile is approximated by that of a cylindrical drop on a fiber, which can be described as an infinite stripe with the same profile in any plane normal to the fiber axis. Such a drop can be considered as a clam shell with an infinite dimension in the direction of the fiber axis. One can suppose that the profiles of the cylindrical and clam-shell drops are close to each other provided that both droplets have equal heights. As an argument in favor of such a conclusion, one can mention that the same similarity occurs for the profiles of cylindrical and axisymmetrical drops of equal heights on a planar surface.[12,13] Consideration of the cylindrical drop on a fiber can also provide information about the roll-up transition. Although a cylindrical drop can be used to approximate the clam-shell one, a film with the same volume can be used to approximate the barrel drop. By calculating and comparing the potential energies of those two configurations of the liquid on the fiber, one can find the transition between the two.

Note that the Laplace pressure is no longer constant if one takes into account the liquid−liquid and liquid−solid interactions. Those interactions can be described in the framework of a macroscopic approach by introducing the disjoining pressure[14] that depends on the distance of the liquid molecules from the solid surface. In this case, it is the sum of the disjoining and Laplace pressures that is constant along the drop surface.

Another, microscopic, approach that accounts for the intermolecular interactions was developed by Ruckenstein et al.[15,16] and applied to the calculation of the droplet shapes on a planar solid surface[12,13,15,16] and of barrel droplets on fibers.[8] The microscopic theory provides in a natural way, without additional assumptions, the microscopic contact angle (θ_0) between the actual drop profile and the solid surface, which depends on the interaction potentials. The theory reveals a rapid change of the curvature of the drop profile in the nanometric range near the solid surface, where the interactions between liquid and solid are strong. This leads to a difference between the microcontact angle (θ_0) between the drop profile and the solid surface and the measurable macroscopic contact angle (θ_m) determined with the wetting angle instrument. The latter represents in reality the angle between the extrapolation of the profile somewhat farther from the leading edge (outside the range of strong interactions between the liquid and the solid) and the surface. θ_m can be evaluated by considering the profile as a part of a circle with the curvature equal to that at the apex of the drop profile.[12,13] Let us note that the distinction between the microscopic and macroscopic contact angles was initially made in ref 16. The microscopic approach is applied in the present paper to the description of a cylindrical droplet on a fiber.

In Section II, the interaction potentials are introduced, and the total potential energy of a system is calculated in Section III. Using the variational minimization of that energy, an equation for the profile is derived in Section IV and solved by quadrature, and an expression for the microcontact angle θ_0 is obtained. Section V is devoted to the finding of the existence conditions of a cylindrical drop on a fiber, which are further used in Section VI to examine the drop shape. The features of the roll-up transition between the cylindrical and the film-like configurations are discussed in Section VII.

II. Potentials of Intermolecular Interactions

A. Interaction between the Molecules of the Liquid. The potential $\phi_{LL}(r)$ of the interaction between the molecules of the liquid is chosen in the form

$$\phi_{LL}(r) = \begin{cases} 0, & r > \eta, \\ -\epsilon_{LL}\left(\dfrac{\sigma_{LL}}{r}\right)^6, & \eta \geq r \geq \sigma_{LL}, \\ \infty, & r < \sigma_{LL}, \end{cases} \tag{1}$$

where r is the distance between the centers of the interacting molecules, $\sigma_{LL} > 0$ and $\epsilon_{LL} > 0$ are the size of the repulsive core and an interaction constant, respectively, and η (a radius of the interaction sphere) is the largest value of r for which the interaction is considered as nonzero. The potential eq 1 is a simplified version of the London-van der Waals potential with a rigid core repulsion

$$\tilde{\phi}_{LL}(r) = \begin{cases} -\epsilon'_{LL}\left(\dfrac{\sigma'_{LL}}{r}\right)^6, & r \geq \sigma'_{LL}, \\ \infty, & r < \sigma'_{LL} \end{cases} \tag{2}$$

which is difficult to use in the variational calculation of the drop shape because of the long-range nature of the potential. Because the London-van der Waals potential decreases rapidly with r, the approximate eq 1 seems reasonable. In ref 8, the relation between ϵ_{LL}, σ_{LL}, and η on one hand and ϵ'_{LL} and σ'_{LL} on the other hand was obtained using the requirement of equality of the total potential energies ϕ_1 and ϕ'_1 of a molecule in the bulk of a homogeneous liquid, calculated using the potentials eq 1 and eq 2, respectively. That relation has the form

$$\frac{\epsilon_{LL}}{\epsilon'_{LL}} = \left(\frac{\sigma'_{LL}}{\sigma_{LL}}\right)^3 (1 - \Delta^3)^{-1} \tag{3}$$

where $\Delta = \sigma_{LL}/\eta$. If, for example, $\eta = 3\sigma_{LL}$, then the following particular choices for parameters ϵ_{LL} and σ_{LL} are obtained: $\sigma_{LL} = \sigma'_{LL}$, $\epsilon_{LL} = (27/26)\epsilon'_{LL}$.

B. Interactions between the Molecules of Liquid and Solid, and Vapor and Solid. It is supposed that the interaction potential between a molecule of liquid and a molecule of solid is equal to the sum of two components, $\phi^l_{LS}(r)$ and $\phi^s_{LS}(r)$, related to the long-range and the short-range interactions. The long-range potential is chosen in a form similar to $\tilde{\phi}_{LL}(r)$

$$\phi^l_{LS}(r) = \begin{cases} -\epsilon_{LS}\left(\dfrac{\sigma_{LS}}{r}\right)^6, & r \geq \sigma_{LS}, \\ \infty, & r < \sigma_{LS}, \end{cases} \tag{4}$$

where $\sigma_{LS} > 0$ and $\epsilon_{LS} > 0$ are the size of the repulsive core and the interaction constant of the liquid−solid interactions, respectively. In what follows, σ_{LS} is used as the unit of length. In real systems, σ_{LS} is of the order of 3 to 4 Å[17] and for definiteness we selected $\sigma_{LS} = 3$ Å.

The total potential $\Phi^l_{LS}(y)$ of a liquid molecule interacting with a fiber through the long-range interactions was calculated in ref 8, where the fiber was considered as an infinite cylindrical solid body of radius R_f with a constant number density (ρ_S) of atoms. The result is

$$\Phi^{l}_{LS}(y) = \frac{\pi\epsilon_{LS}\rho_S\sigma^6_{LS}}{24(R_f+y)(R_f^2-y^2)^2}\left\{(7R_f^2+y^2)\times\left[E\left(\frac{\pi}{4},-\frac{4R_fy}{(R_f-y)^2}\right)+E\left(\frac{3\pi}{4},-\frac{4R_fy}{(R_f-y)^2}\right)\right]-(R_f+y)^2\left[F\left(\frac{\pi}{4},-\frac{4R_fy}{(R_f-y)^2}\right)+F\left(\frac{3\pi}{4},-\frac{4R_fy}{(R_f-y)^2}\right)\right]\right\} \quad (5)$$

where $y > R_f$ is the distance of a molecule from the fiber axis, and $F(\phi, m)$ and $E(\phi, m)$ are the elliptic integrals of the first and second kind, respectively.[18] In the limiting case $R_f \rightarrow \infty$ the potential $\Phi^{l}_{LS}(y)$ coincides with that of a molecule of liquid interacting with a semi-infinite solid.

Potential eq 5 decreases rapidly within several hard core radii from the fiber surface and for $R_f \gg \sigma_{LS}$ can be approximated with high accuracy by the power law function

$$\Phi^{l}_{LS}(h) = -\frac{\pi}{6}\epsilon_{LS}\sigma^3_{LS}\rho_S\frac{k}{\left(1+\frac{h}{\sigma_{LS}}\right)^{\nu}} \quad (6)$$

where $h = y - R_f - \sigma_{LS}$ and k and ν are constants (for given R_f).[8] For example, for $R_f = 100\sigma_{LS} \simeq 30$ nm, one has $\nu = 3.01712$, and $k = 0.9926$.[8]

The short-range interactions between liquid and solid molecules, such as the acid−base ones, decrease rapidly (exponentially) after distances of the order of 1 nm from the liquid−solid interface.[7,19] Hence, the total potential energy $\Phi^{s}_{LS}(h)$ of the liquid molecule due to those interactions can be approximated by the potential[8]

$$\Phi^{s}_{LS}(h) = \begin{cases} -\epsilon^{s}_{LS}, & h = 0, \\ 0, & h > 0 \end{cases} \quad (7)$$

where ϵ^{s}_{LS} is a constant.

Combining the potentials of eqs 6 and 7, one obtains the total potential, $\Phi_{LS}(h)$, of a molecule of liquid interacting with a fiber

$$\Phi_{LS}(h) = \begin{cases} \Phi^{l}_{LS}(0) + \Phi^{s}_{LS}(0), & h = 0, \\ \Phi^{l}_{LS}(h), & h > 0 \end{cases} \quad (8)$$

The interaction between the molecules of vapor (gas) and solid has in most cases only a long-range component, which, for low-density vapors, is determined only by the molecules adsorbed on the solid surface ($h = 0$). The potential $\Phi_{VS}(h)$ of that interaction can be written in the form

$$\Phi_{VS}(h) = \begin{cases} \Phi^{l}_{VS}(0), & h = 0 \\ 0, & h > 0 \end{cases} \quad (9)$$

where the potential $\Phi^{l}_{VS}(0)$ has the same form as $\Phi^{l}_{LS}(0)$ given by eq 6, where ϵ_{LS} and σ_{LS} have to be replaced by ϵ_{VS} and σ_{VS}, respectively.

III. Potential Energy of the System

If a vapor (gas) that surrounds a drop has a low density, one can neglect the vapor−vapor and vapor−liquid potential energies in the calculation of the total potential energy (U_{total}) of the system and take into account only the interaction of the adsorbed vapor molecules with the solid. The interaction energy of the molecules of the solid between themselves will be considered constant and will also be excluded from consideration. The possible changes of the latter energy caused by the restructuring of the surface molecules of the solid due to their interaction with the molecules of liquid or vapor can be included into the corresponding solid−liquid and solid−vapor interactions. Under those assumptions, U_{total} can be written in the form

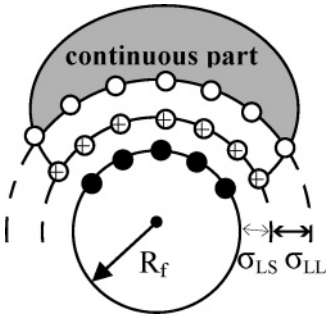

Figure 2. Cross-section of a cylindrical drop on a fiber. The filled and crossed circles represent the molecules on the fiber surface and the molecules of the first (closest to the solid surface) layer of liquid molecules, respectively. Beginning with the second layer (open circle) the liquid is considered as a continuous medium.

$$U_{total} = U_{LL} + U_{LS} + U_{VS} \quad (10)$$

where U_{LL} and U_{LS} are the potential energies due to the interactions of the molecules of liquid between themselves and with those of the fiber, respectively, and U_{VS} is a potential energy due to the interactions between the molecules of the vapor and the fiber.

A. The Potential Energy of a Drop. The model used most frequently for a liquid considers the liquid as a continuous medium characterized by a constant macroscopic number density (ρ_L) of molecules.[5,7,16] Such a continuous picture is not valid in the very vicinity of the fiber surface where the interactions of the liquid molecules with the fiber are the strongest. Because of these interactions, the liquid molecules closest to the fiber surface are rearranged in a layer "sticked" to the fiber surface, which will be assumed to be a monolayer separated from the surface by a distance σ_{LS}. The remainder of the drop is separated from the first layer by a distance, σ_{LL}, and is assumed to be a continuous medium of constant density (see Figure 2).

Assuming that the size of the droplet is much larger than the radius η of the range of the liquid−liquid interactions, the energy U_{LL} can be represented in the form[8]

$$U_{LL} = -K_vV + K_sS_{LV} + K'_sS_{LS} \quad (11)$$

where V, S_{LV}, and S_{LS} are the total volume of the droplet and the surfaces of the liquid−vapor and liquid−solid interfaces, respectively

$$K_v = \frac{2\pi}{3}\epsilon_{LL}\sigma^3_{LL}\rho^2_L(1-\Delta^3)$$

$$K_s = \frac{2\pi}{3}\epsilon_{LL}\sigma^4_{LL}\rho^2_L\left[\frac{17}{16}-\frac{3}{8}\Delta^2+\frac{1}{2}\Delta^3-\frac{3}{16}\Delta^4-\frac{\rho_{LV}}{\sigma_{LL}\rho_L}(1-\Delta^3)\right]$$

$$K'_s = \frac{2\pi}{3}\epsilon_{LL}\sigma^4_{LL}\rho^2_L\left[\frac{17}{16}-\frac{3}{8}\Delta^2+\frac{1}{2}\Delta^3-\frac{3}{16}\Delta^4-\frac{\rho_{LS}}{\sigma_{LL}\rho_L}(1-\Delta^3)\right] \quad (12)$$

and ρ_{LV} and ρ_{LS} are the surface densities of the liquid at the liquid−vapor and liquid−solid interfaces, respectively.

To calculate the interaction energy, U_{LS}, let us note that the molecules closest to the solid layer are affected by both long-range and short-range interactions with the fiber, which are represented by the potential eq 8 for $h = 0$. The molecules of the continuous part of the drop do not exhibit short-range interactions.

Under the above assumptions, the energy (U_{LS}) is given by

$$U_{LS} = \rho_{LS}\Phi_{LS}(0)S_{LS} + \int_{V_{cont}} \rho_L \Phi^l_{LS}(h)\mathrm{d}V \qquad (13)$$

where S_{LS} is the contact area between the droplet and the fiber, and V_{cont} denotes the volume of the continuous part of the droplet. The latter can be written as the difference between the drop volume (V) and the volume (V_g) of the gap between the first layer and the continuous part of the droplet that is approximately equal to $V_g = \sigma_{LL}S_{LS}$, that is, $V_{cont} = V - S_{LS}\sigma_{LL}$. Then the second term in the right-hand side of eq 13 becomes

$$\int_{V_{cont}} \rho_L \Phi^l_{LS}(h)\mathrm{d}V = \int_V \rho_L \Phi^l_{LS}(h)\mathrm{d}V - \int_{V_g} \rho_L \Phi^l_{LS}(h)\mathrm{d}V \simeq \int_V \rho_L \Phi^l_{LS}(h)\mathrm{d}V - \rho_L \sigma_{LL}\Phi^l_{LS}(\sigma_{LL})S_{LS} \qquad (14)$$

Consequently

$$U_{LS} \simeq \int_V \rho_L \Phi^l_{LS}(h)\mathrm{d}V + [\rho_{LS}\Phi_{LS}(0) - \rho_L\sigma_{LL}\Phi^l_{LS}(\sigma_{LL})]S_{LS} \qquad (15)$$

B. Potential Energy of the Vapor−Solid Interactions. As already mentioned in Section II.B, only the contribution of the adsorbed vapor molecules to the vapor−solid potential energy will be taken into account. Using the potential eq 9 and denoting the surface density of the vapor molecules on the solid surface ρ_{VS}, we can write the potential energy (U_{VS}) of the vapor−solid interactions in the form

$$U_{VS} = \rho_{VS}(S_{solid} - S_{LS})\Phi^l_{VS}(0) \qquad (16)$$

where S_{solid} is the total area of the solid surface and S_{LS} is the area of the liquid−solid interface.

Using eqs 11, 15, and 16 and omitting the constant term proportional to S_{total} in the last equation, the following expression for the total potential energy of the system is obtained

$$U_{total} = -K_v V + K_s S_{LV} + \int_V \rho_L \Phi^l_{LS}(h)\mathrm{d}V + K_s b S_{LS} \qquad (17)$$

where

$$b = \frac{K'_s}{K_s} + \frac{1}{K_s}[\rho_{LS}\Phi_{LS}(0) - \rho_L\sigma_{LL}\Phi^l_{LS}(\sigma_{LL}) - \rho_{VS}\Phi^l_{VS}(0)] \qquad (18)$$

Equation 17 provides the basis for the analysis of the drop characteristics (existence, shape, etc.).

IV. Equation for the Profile of a Cylindrical Drop

In Figure 3 two possible profiles of a cylindrical drop on a fiber in the plane perpendicular to the axis of the fiber are presented together with the polar coordinate system used in the calculations. The surface of the cylindrical drop is obtained by translating the profile along the axis of the fiber. We consider a drop on a bare surface; thefore, the leading edge of the drop is located just on the fiber surface.

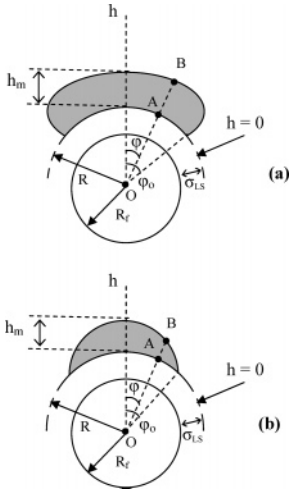

Figure 3. Characteristic profiles of a cylindrical drop in a plane normal to the fiber axis: (a) microcontact angle θ_0 is larger than 90°; (b) θ_0 is smaller than 90°.

To provide a unique description for both shapes (Figure 3a and b), the equation of the drop profile is chosen in the present paper in the form $\phi = \phi(h)$, and only the part of the profile for which $\phi \geq 0$ will be examined further.

The equation of the drop profile can be derived using the variational minimization of the total potential energy (U_{total}) of the drop defined by eq 17 assuming the constancy of the drop volume. The derivation details are given in Appendix A. The equation for the profile has the form

$$\frac{(R+h)\phi_{hh} + 2\phi_h + (R+h)^2\phi_h^3}{[1 + (R+h)^2\phi_h^2]^{3/2}} - a_1\Phi^l_{LS}(h) = \lambda_c \qquad (19)$$

where the subscript h means differentiation with respect to h, $R = R_f + \sigma_{LS}$, $a_1 = \rho_L/K_s$, and λ_c is a constant dependent on the drop volume. The first term of eq 19 represents the curvature $\kappa(h)$ of the drop profile in polar coordinates.

The boundary conditions for eq 19 have the form

$$\phi|_{h=h_m} = 0 \qquad (20)$$

$$\phi_h|_{h=0} = -\frac{1}{R}\cot\theta_0 \qquad (21)$$

where h_m is the droplet height at its apex (Figure 3) and θ_0 is the microcontact angle (θ_0 is defined as the angle between the tangents to the profiles of the fiber and profile of the drop at the point of contact). Note that the height h_m is not given and can be found using the known value of the drop volume.

Eq 21 follows from the fact that in polar coordinates the angle α that the curve $\phi = \phi(r)$ makes with the circle $r = R$ is given by the expression

$$\tan\alpha = -\frac{1}{R\phi_r} \qquad \left(\phi_r \equiv \frac{\mathrm{d}\phi}{\mathrm{d}r}\right) \qquad (22)$$

and that in our case $\phi_r = \phi_h$. The expression for angle θ_0 is obtained from the so-called transversality conditions,[20] which allows one to connect θ_0 to the microscopic parameters of the interaction potentials. The result is (see Appendix A)

$$\cos\theta_0 = -b \qquad (23)$$

where b is provided by eq 18.

It should be noted that the above expression for the microcontact angle (θ_0) was obtained from pure microscopic considerations. Angle θ_0 depends on the parameters of the intermolecular interactions and on the fiber radius, R_f.

The solution of eq 19 for the boundary conditions eqs 20 and 21 is (see Appendix B)

$$\phi(h) - \phi_0 = \int_0^h \frac{\Psi(h)}{(R+h)\sqrt{1-\Psi^2(h)}}\,dh \tag{24}$$

where $\phi_0 \equiv \phi(0)$ (Figure 3)

$$\Psi(h) = \frac{1}{R+h}\left\{-R\cos\theta_0 + \frac{\lambda_c}{2}h(h+2R) - a[D(h) - D(0)]\right\} \tag{25}$$

$$a = \frac{1}{4K_1}\frac{\epsilon_{LS}\rho_S}{\epsilon_{LL}\rho_L}\left(\frac{\sigma_{LS}}{\sigma_{LL}}\right)^4 \tag{26}$$

$$K_1 = \frac{17}{16} - \frac{3}{8}\Delta^2 + \frac{1}{2}\Delta^3 - \frac{3}{16}\Delta^4 - \frac{\rho_{LV}}{\sigma_{LL}\rho_L}(1-\Delta^3) \tag{27}$$

and

$$D(h) = -\frac{a_1}{a}\int \Phi_{LS}^1(h)(R+h)dh \tag{28}$$

The explicit expressions for constants ϕ_0 and λ_c and the function $D(h)$ are provided in Appendix B. To find all of the unknown parameters (ϕ_0, λ_c, and h_m) it is necessary to add to eqs 20 and 21 the equation for the drop volume $V = 2\int_0^{h_m}(R+h)\phi dh$. Substituting $\phi(h)$ given by eq 24 and changing the order of integration one obtains

$$V = -\int_0^{h_m}\frac{(h^2+2Rh)\Psi(h)}{\sqrt{1-\Psi^2(h)}}\,dh \tag{29}$$

V. Existence of a Cylindrical Drop on a Bare Surface of a Fiber

The first necessary condition for the existence of a drop on a bare surface follows from eq 23 and has the simple form $|b| \le 1$. It establishes (through eq 18) a restriction for the values of the microscopic parameters for which a cylindrical drop can be formed on a surface. If $|b| > 1$, a cylindrical drop cannot exist. It should be noted that the restriction $|b| < 1$ (or, equivalently, $|\cos\theta_0| < 1$) differs from the traditional one, which implies $|\cos\theta_m| < 1$.

A second general necessary condition results from the fact that the integral on the right-hand side of eq 24 has meaning only if the function $\Psi(h)$ satisfies the inequality

$$|\Psi(h)| < 1, (0 < h < h_m) \tag{30}$$

The function $\Psi(h)$ depends on the fiber radius (R_f), the drop height (h_m), the microcontact angle (θ_0), and microparameter a and satisfies the conditions $\Psi(h_m) = -1$, $\Psi(0) = -\cos\theta_0$. For any given values of the parameters, $\Psi(h)$ (eq 25) can have one of the three behaviors shown in Figure 4a. However, because only the first satisfies restriction eq 30, a cylindrical droplet will exist only for those values of the parameters for which $\Psi(h)$ exhibits the first behavior.

To examine the consequences of the second necessary condition in more detail, let us first consider the case in which

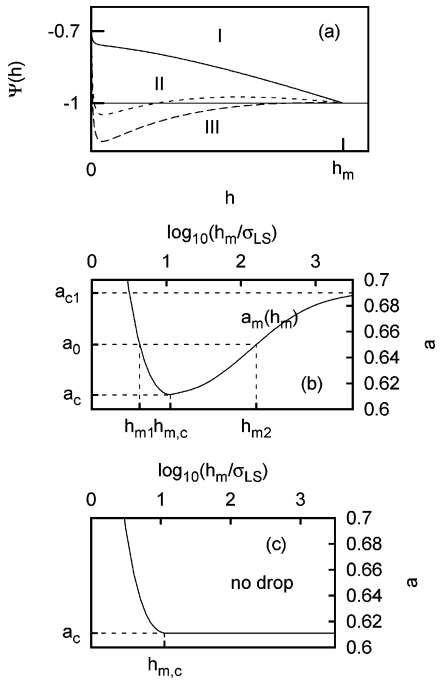

Figure 4. (a) Three types of behavior of the function $\Psi(h)$ given by eq 25. A cylindrical drop on the fiber exists only for those values of the parameters that provide the first type of behavior. (b) The critical curve $a = a_m(h_m)$ that divides the $h_m - a$ plane into two domains for which the second necessary condition given by inequality 30 is not fulfilled (above the curve) and fulfilled (below the curve). (c) The final critical curve $a_c(h_m)$.

R_f (= $100\sigma_{LS}$) and θ_0(= 45°) are fixed and only h_m and a are variables. The analysis of the behavior of function $\Psi(h)$ shows that inequality 30 is valid only in a domain of the $h_m - a$ plane below a critical curve $a = a_m(h_m)$ (see Figure 4b), which exhibits a minimum $a = a_c = 0.613$ at $h_m = h_{m,c} = 11.2\sigma_{LS}$ and reaches the asymptotic value $a = a_{c1} = 0.692$ for $h_m \to \infty$. If $a < a_c$, the drop can have any height. If a specific value a_0 of the parameter a lies between a_c and a_{c1} (e.g., $a_0 = 0.65$), then the second necessary condition is satisfied by h_m values smaller than $h_{m,1} = 4.44\sigma_{LS}$ or larger than $h_{m,2} = 147.77\sigma_{LS}$. The analysis of the shape of the drop profile (Section VI) shows that for $h_m > h_{m,2}$ the angular length of the droplet (the angle ϕ_0 of Figure 3) is larger than 180° and therefore those shapes do not have any physical meaning. As a result, the actual critical curve in the $h_m - a$ plane has the form presented in Figure 4c. The critical value (a_c) depends on the radius (R_f) of the fiber and on the microcontact angle (θ_0). As R_f increases, a_c decreases and for $R_f \to \infty$ (planar surface) acquires the value $a_c = 0.5857$.

By performing similar analyses for other values of θ_0, one can plot a_c against θ_0 in a $\theta_0 - a$ plane (see Figure 5). The curve $a = a_c(\theta_0)$ separates the domains of restricted and unrestricted droplet heights for $R_f = 100\sigma_{LS}$. The pairs (θ_0, a) for which the droplet height h_m can have any value lie below that curve. In the domain located above the curve, the drop height can take only values $h_m < h_{m,1}$.

VI. Shape of the Drop Profile and the Contact Angle

In this section, the shape of the drop profile will be examined for various values of microcontact angle θ_0 and parameter a, which characterizes the liquid−liquid and liquid−solid interactions. Because of the strong interaction between solid and liquid near the liquid−solid interface, the curvature and slope of the drop change rapidly with the distance from the solid. For a drop on a planar surface, it was shown[12,13] that the main change of

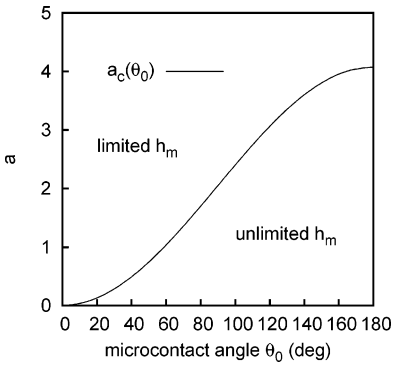

Figure 5. Dependence of the critical values a_c and a_{c1} of the parameter a on the microcontact angle θ_0 for $R_f = 100\sigma_{LS} \approx 30$ nm. The solid line ($a = a_c(\theta_0)$) divides the $\theta_0 - a$ plane into domains of unlimited (below the solid line) and limited (above solid line) heights.

the curvature occurs in a range of about 10 to $40\sigma_{LS} \simeq 3$ to 12 nm. At larger distances from the solid, the curvature of the profile remains almost constant. The slope of the profile also changes rapidly in that nanometric range. The microcontact angle (θ_0) cannot be determined with the conventional equipment employed for wetting angle measurements which cannot "see" what happens in the very vicinity of the solid surface. The experimentally measured angle (θ_m) is in reality an extrapolation of the profile slope from a macroscopic distance from the leading edge up to the solid surface. A useful approximation of the drop profile away from the solid surface is a circular shape with a radius equal to the curvature radius of the profile at the droplet apex. For a drop on a planar solid, the angles θ_0 and θ_m are represented in Figure 6a. For a drop on a fiber, the angles θ_0 and θ_m can be defined in a similar way (see Figures 6b and c). To calculate angle θ_m for the latter case one can use the expression

$$\cos\theta_m = \frac{R_m^2 + R^2 - d^2}{2R_m R} \tag{31}$$

where $R_m = 1/|\kappa(h_m)|$ is the curvature radius at the drop apex, and $d = R - R_m + h_m$. (Equation 31 follows from the application of the cosine theorem to the triangle OAO' of Figure 7.) The curvature $\kappa(h)$ can be found from eq 19 and has the form

$$\kappa(h) = \lambda_c + a_1\Phi_{LS}^{l}(h) \tag{32}$$

where λ_c is given by B.14 and $\Phi_{LS}^{l}(h)$ by eq 6. One can thus obtain a relation between cos θ_m and cos θ_0. For a drop for which $\sigma_{LS} \ll h_m \ll R$, one obtains the simple expression

$$\cos\theta_m = \left(1 + \frac{h_m}{2R}\right)\cos\theta_0 + \frac{ak}{\nu - 1} - \frac{h_m}{2R}\left(1 - \frac{ak}{\nu - 1}\right) \tag{33}$$

which for $R \to \infty$ leads to the equation

$$\cos\theta_m = \cos\theta_0 + \frac{a}{2} \tag{34}$$

obtained previously for a drop on a planar surface.[12,13]

The specific features of the cylindrical drop profile on the fiber depend on several factors, including the distance of the point (θ_0, a) from the critical line and the drop volume. Taking as an example a fiber of radius $R_f = 100\sigma_{LS}$, the typical profiles of a small droplet of volume $V = 3.63 \times 10^3\sigma_{LS}^2 \simeq 1.0 \times 10^2$ nm^2 per unit length of the drop are presented in Figure 8 for a = 0.61 and various values of the microcontact angle θ_0 from the domain of unlimited heights. The selected value of a is close to the critical value $a_c = 0.613$ for $\theta_0 = 45°$. Therefore, the plot of the profile (solid line) in Figure 8a corresponds to a point (θ_0, a) in the very vicinity of the critical line $a = a_c(\theta_0)$ (see Figure 5). The dashed curve represents the circular approximation for the drop profile. In the case considered, the circle has no intersection with the fiber and most of the droplet profile and the profile of the fiber can be considered as approximately concentric circles. This case is similar to that of a planar droplet on a planar solid surface,[12,13] which occurs when the point (θ_0, a) is located near the critical line. For this reason, the above drop on the fiber can be considered as a quasi planar one.

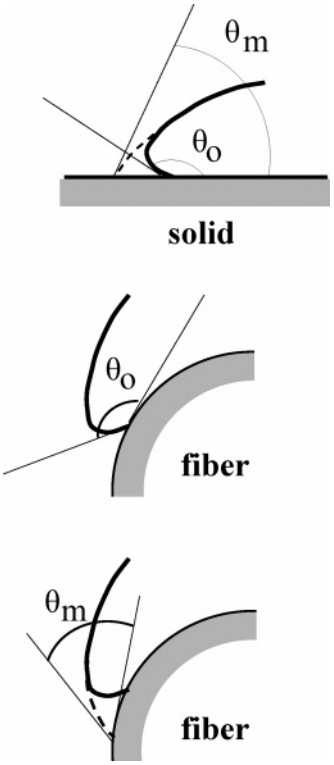

Figure 6. Microscopic, θ_0, and macroscopic, θ_m, contact angles for the drop profile on a planar solid (a) and fiber (b, c). The circular approximation for the profile is represented by the dashed lines.

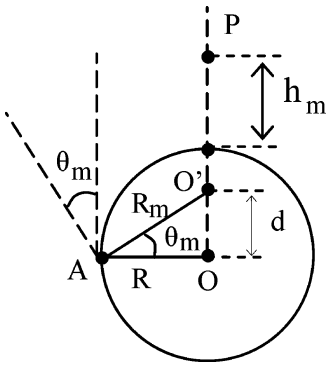

Figure 7. Auxiliary plot for the calculation of macroscopic contact angle θ_m. O and O' are, respectively, the centers of a fiber of radius R and a circle with a radius R_m equal to the curvature radius at the drop apex P. The latter circle is not shown in the figure.

When θ_0 increases, the angular length ϕ_0 of the droplet becomes smaller, the droplet height increases, and the approximation of the drop profile by a circular one becomes better. As a consequence, the approximate and exact curves in Figure

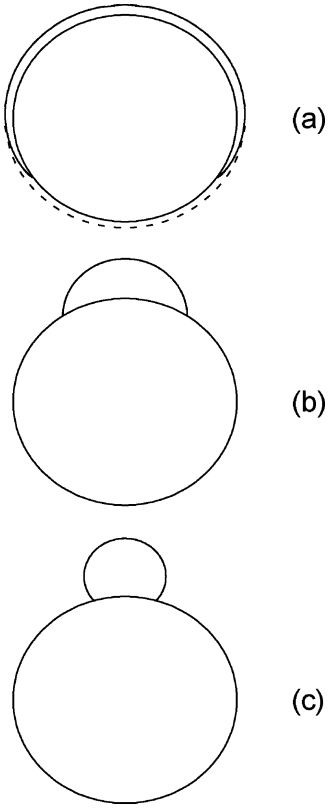

Figure 8. Profiles of a small drop of volume $V = 3.63 \times 10^3 \sigma_{LS}^2 \simeq 1.0 \times 10^2$ nm^2 per unit length for several values of the microcontact angle θ_0 (solid lines) and $a = 0.612$: (a) $\theta_0 = 45°$; (b) $\theta_0 = 75°$; (c) $\theta_0 = 135°$. The dashed line on figure a represents a circular profile with the same height (h_m) as the original one and with a radius equal to the curvature radius of the original profile at the drop apex. The same approximations for figures b and c almost coincide with the profiles of the drops. There is a difference at the leading edge that cannot be detected by eyes. All of the profiles correspond to the points (θ_0, a) in the domain of unlimited height, the point (θ_0, a) for profile a being located in the very vicinity of the critical line.

8b and c become indistinguishable by eye. However, in the very vicinity of the fiber surface, the circular approximation does not coincide with the exact solution and therefore the microscopic and macroscopic contact angles have different values. For instance, for the profiles shown in Figure 8 b and c for $\theta_0 = 75$ and 135° the angles (θ_m) are 55.9 and 113.9°, respectively. For a similar droplet on a planar surface the angles (θ_m) were 55 and 113.7°, respectively, almost the same as on the fiber. The profiles of a larger droplet ($V = 4.1 \times 10^4 \sigma_{LS}^2 \simeq 1.1 \times 10^3$ nm^2) are presented in Figure 9. These profiles cannot be considered as quasi planar. The macroscopic contact angles (θ_m) are practically the same as those for the small droplet.

When the pair (θ_0, a) lies above the critical line $a = a_c(\theta_0)$ (Figure 5) the droplet height can acquire only values $h_m < h_{m,1}$ and the droplet has a quasi planar shape when $h_m \rightarrow h_{m,1}$. It should be noted that $h_{m,1}$ in the cases considered above is small ($h_{m,1} < 5$ Å), and therefore the applicability of the theory is questionable.

VII. Roll-Up Transition

For the complete examination of the existence conditions for a cylindrical drop on a fiber, it is necessary to take into account its possible transformation to a film that covers the fiber. The latter transformation takes place if the potential energy for a film is smaller than that for a cylindrical droplet, provided that both the film and the droplet have the same volume (V) per unit length.

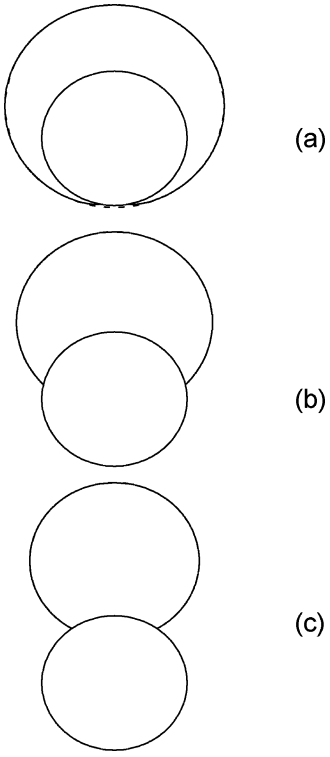

Figure 9. Profiles of a relatively large drop of a volume per unit length $V = 4.1 \times 10^4 \sigma_{LS}^2 \simeq 1.1 \times 10^3$ nm^2 for several values of microcontact angle θ_0 (solid lines) and $a = 0.612$: (a) $\theta_0 = 45°$; (b) $\theta_0 = 75°$; (c) $\theta_0 = 135°$. All of the other notations are the same as those in Figure 8.

The total potential energy, U_{total}^{cyl}, of a cylindrical droplet is provided by eq 17, where the drop volume and areas of the liquid−solid and liquid−vapor interfaces can be calculated using eq A.1 from Appendix A.

For a film, the total potential energy can be calculated in the same way as for a cylindrical drop and the result is

$$U_{total}^{f} = -K_v V_f + K_s S_{LV}^{f} + \int_{V_f} \rho_L \Phi_{LS}^{l}(h) dV + K_s b S_{LS}^{f} \quad (35)$$

where V_f, S_{LV}^{f}, and S_{LS}^{f} are the volume and the areas of liquid−vapor and liquid−solid interfaces of the film, respectively. Simple geometrical considerations give

$$S_{LV}^{f} = 2\pi(h_f + 2R)$$

$$S_{LS}^{f} = 2\pi R$$

$$\int_{V_f} \rho_L \Phi_{LS}^{l}(h) dV = 2\pi\rho_L \int_0^{h_f} (R + h)\Phi_{LS}^{l}(h) dh \quad (36)$$

In eq 36, h_f is the film thickness which for a volume $V_f = V$ is given by

$$h_f = \sqrt{R^2 + \frac{V}{\pi}} - R$$

Employing eqs 17 and 35, the difference of potential energies $U_{total}^{f} - U_{total}^{cyl} \equiv \Delta U$ can be represented in the form

$$\frac{1}{2K_s}\Delta U = \pi(h_f + R) - \int_0^{h_m}\sqrt{1+(R+h)^2\phi_h^{\,2}}\,dh + Rb(\pi - \phi_0) - a\left\{\pi[D(h_f) - D(0)] - \int_0^{h_m}\frac{k(R+h)}{\left(1+\frac{h}{\sigma_{LS}}\right)^{\nu}}\phi\,dh\right\} \quad (37)$$

where the functions $\phi \equiv \phi(h)$ and $D(h)$ are provided by eqs 24 and B.8, respectively. In Figure 10 the difference ΔU is plotted as a function of the droplet volume for $\theta_0 = 45°$ for various values of the parameter a from the domain of unlimited heights ($a < a_c = 0.613$) and $R = 100\sigma_{LS}$. For $a > a_{lim} \simeq 0.536$, ΔU changes sign at a volume V_c, which depends on a. Therefore, for $V > V_c$, U^{f}_{total} is smaller than U^{cyl}_{total} and the film configuration is more stable than the cylindrical droplet. If $a < a_{lim}$ the potential energy of the cylindrical drop is smaller than that of the film for any value of the volume, that is, the cylindrical configuration is always stable.

Experimental data[1] show that the critical volume (V_c) of a drop at which the roll-up transition occurs increases with increasing macroscopic contact angle. In Figure 11 the θ_0-dependence of the critical volume is presented for two values of a and for a fiber with $R_f = 20\sigma_{LS}$. (The θ_m-dependence is qualitatively similar). For each a, the roll-up transition takes place only in a narrow range of microcontact angles ($\theta_{0,1} < \theta_0 < \theta_{0,2}$) from the domain of unlimited heights. Outside this region, the cylindrical droplets are energetically preferable at any drop size. In the range $\theta_{0,1} < \theta_0 < \theta_{0,2}$, the volume ($V_c$) increases rapidly with increasing θ_0. Such a behavior coincides qualitatively with the experimental observations.[11] However, experiment provides a much wider (but also restricted) range

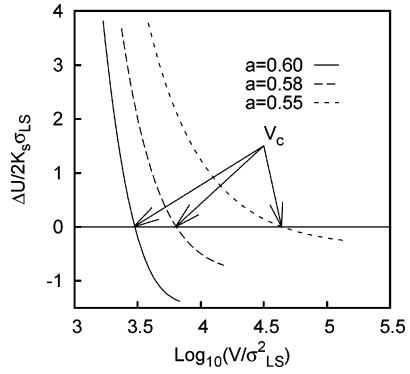

Figure 10. The difference (ΔU) between the potential energies of the system for a film and a cylindrical drop of the same volume (V) as a function of V for several values of parameter a. The microcontact angle is equal to $\theta_0 = 45°$. V_c represents the critical volume at which the roll-up transition occurs.

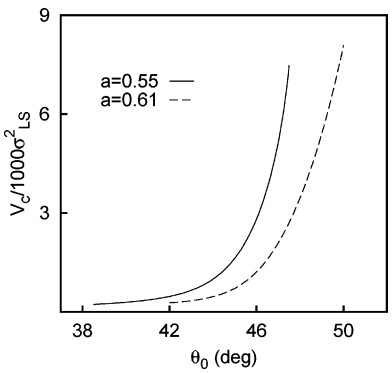

Figure 11. Dependence of the critical volume (V_c) on microcontact angle θ_0 for several values of parameter a.

of contact angles where the roll-up transition occurs. The possible reason for such a difference is that the experimental data were obtained for finite-size drops (barrel and clam-shell), whereas the theory considers infinite sizes for both the barrel and the clam-shell drops. The smaller the value of the parameter a, the smaller is the angle θ_0 for which the roll-up transition occurs. Note that the range of existence of the roll-up transition increases with decreasing R_f. For example, for $R_f = 20\sigma_{LS}$ and $a = 0.61$ the difference $\theta_{0,2} - \theta_{0,1}$ is 8.0°, whereas for $R_f = 100\sigma_{LS}$ it is 4.2^0

VIII. Discussion and Summary

In this paper, a microscopic approach is applied to the description of a cylindrical drop on a fiber and to the transition from a drop to a film covering the fiber (roll-up transition). Considering the cylindrical drop as a limiting case of a clam-shell one, and the film as a limiting case of a barrel drop, the obtained analytical results can be related to the barrel-drop−clam-shell drop transition (roll-up transition), which was treated before only numerically in the framework of a macroscopic approach. The analysis of the equation for the drop profile reveals that the drop existence conditions depend on the value of microparameter a, eq 26, which incorporates the microscopic parameters of liquid−liquid, solid−liquid, and solid−gas interactions as well as the liquid and the solid densities. For each value of microcontact angle θ_0, a critical value, a_c, exists which separates two ranges of possible drop heights. In the first range $a < a_c$, and the drop can have any height (h_m) and volume. In the second range $a > a_c$, and the drop height is upper bounded by some value, h_{m1}.

The locus of the points (θ_0, a_c) (critical line) divides the $\theta_0 - a$ plane into two domains shown in Figure 5, each of them corresponding to one of the ranges mentioned above. The shape of the drop profile for a given fiber radius (R_f) depends on the drop size, microcontact angle θ_0, and parameter a. If the point (θ_0, a) belongs to the domain of unlimited heights (below the curve $a = a_c(\theta_0)$ in Figure 5) and lies in the very vicinity of the critical line, then the small droplets have a quasi planar shape, that is, most of the drop profile is located on a circle concentric with the profile of the fiber. However, the larger droplets do not possess such a shape (compare Figures 8a and 9a). If the point (θ_0, a) lies far from the critical line, then the drop shape is close to a circular one. In all cases, the values of the macrocontact (θ_m) and microcontact (θ_0) angles do not coincide. The difference between θ_0 and angle θ_m (the angle determined with the conventional wetting angle instrument) is a consequence of the strong interactions between the solid and liquid near the leading edge of the drop. Near the leading edge there is a very strong variation of the drop curvature, whereas somewhat farther from the leading edge, where the interactions with the solid are not as strong, the curvature becomes almost constant. The wetting angle instrument can determine angles in the macroscopic range and not in the microscopic range near the leading edge. For this reason, the measured wetting angle is an extrapolation of the slope of the drop from some distance from the leading edge to the solid surface.

When the point (θ_0, a) is located in the domain of limited droplet heights corresponding to the second range of drop existence (above the curve $a = a_c(\theta_0)$ in Figure 5) the drops become quasi planar when h_m is close to h_{m1}.

Analysis of the roll-up transition shows that for given values of a and R_f it occurs only if the microcontact angle lies in a narrow interval $\theta_{0,1} < \theta_0 < \theta_{0,2}$, $\theta_{0,1}$ and $\theta_{0,2}$ being functions of R_f and a, and the drop volume is larger than some critical

value, V_c. Note that the point ($\theta_{0,1}$, a) is located near the critical curve in Figure 5, and the difference between $\theta_{0,2}$ and $\theta_{0,1}$ increases with decreasing R_f. If the microcontact angle θ_0 lies outside the interval ($\theta_{0,1}$, $\theta_{0,2}$), then the roll-up transition does not occur for any drop volume.

Acknowledgment. We are grateful to Ilya G.Berim for his help in numerical calculations.

Appendix A. Derivation of the Equation for the Drop Profile

Expressions for drop volume V, surfaces S_{LV} and S_{LS}, and the integral $\int_V \rho_L \Phi^l_{LS}(y)\, dV$ on the right-hand side of, which are necessary to find the total potential energy, U_{total}, have the form (all quantities are given per unit length of the drop)

$$V = 2\int_0^{h_m}(R+h)\phi\, dh,\ S_{LV} = 2\int_0^{h_m}\sqrt{1+(R+h)^2\phi_h^2}\, dh,\ S_{LS} = 2R\phi_0 = -2R\int_0^{h_m}\phi_h\, dh,\ \int_V \rho_L \Phi^l_{LS}(y)\, dV = 4\pi\rho_L\int_0^{h_m}\Phi^l_{LS}(h)(R+h)\phi\, dh \quad (A.1)$$

where $R = R_f + \sigma_{LS}$, $\phi_h \equiv d\phi/dh$, and h_m is the droplet height. The angular length, ϕ_0, of the drop

$$\phi_0 = -\int_0^{h_m}\phi_h\, dh = -\phi(h)|_0^{h_m} = \phi(0) \quad (A.2)$$

follows from the obvious fact that $\phi(h_m) = 0$ (Figure 3). The total potential energy is given by

$$U_{total} = \int_0^{h_m} f(h,\phi,\phi_h)dh \quad (A.3)$$

where

$$f(h,\phi,\phi_h) = 2K_s\{[-a_0 + a_1\Phi^l_{LS}(h)](R+h)\phi + \sqrt{1+(R+h)^2\phi_h^2} - bR\phi_h\} \quad (A.4)$$

$$a_0 = \frac{K_v}{K_s} \qquad a_1 = \frac{\rho_L}{K_s} \quad (A.5)$$

and

$$b = \frac{K'_s}{K_s} + \frac{1}{K_s}[\rho_{LS}\Phi_{LS}(0) - \rho_L\sigma_{LL}\Phi^l_{LS}(\sigma_{LL}) - \rho_{VS}\Phi^l_{VS}(0)] \quad (A.6)$$

From eqs 6, 7, and 8 one has

$$\Phi_{LS}(0) = -\frac{\pi}{6}\epsilon_{LS}\rho_S\sigma^3_{LS}k - \epsilon^s_{LS} \qquad \Phi^l_{VS}(0) = -\frac{\pi}{6}\epsilon_{VS}\rho_S\sigma^3_{VS}k \quad (A.7)$$

and

$$\Phi^l_{LS}(\sigma_{LL}) = -\frac{\pi}{6}\epsilon_{LS}\rho_S\sigma^3_{LS}\frac{k}{\left(1+\frac{\sigma_{LL}}{\sigma_{LS}}\right)^\nu} \quad (A.8)$$

Because of the dependence of potentials $\Phi_{LS}(h)$, $\Phi^l_{LS}(h)$, and $\Phi^l_{VS}(0)$ on the radius of the fiber, R_f, b is also R_f-dependent.

In the case of constant drop volume, the equation of the drop profile can be obtained by the variational minimization of the functional

$$\int_0^{h_m} f(h, x, x_h)dh + 2\lambda\int_0^{h_m}(R+h)\phi\, dh \quad (A.9)$$

where λ is a Lagrange multiplier for the drop volume. The latter functional can be rewritten in the following more convenient form

$$\int_0^{h_m} F(h,\phi,\phi_h)dh \quad (A.10)$$

where

$$F(h,\phi,\phi_h) = [\lambda_c + a_1\Phi^l_{LS}(h)](R+h)\phi + \sqrt{1+(R+h)^2\phi^2_h} - bR\phi_h \quad (A.11)$$

and

$$\lambda_c = \frac{\lambda}{K_s} - a_0 \quad (A.12)$$

The functional $F(h,\phi,\phi_h)$ in A.11 is obtained by dividing the functional of A.9 with the nonzero coefficient $2K_s$.

Employing the standard calculus of variations,[20] the following differential equation for the profile is obtained

$$\frac{(R+h)\phi_{hh} + 2\phi_h + (R+h)^2\phi_h^3}{[1+(R+h)^2\phi_h^2]^{3/2}} - a_1\Phi^l_{LS}(h) = \lambda_c \quad (A.13)$$

Because the apex of the droplet and the contact point of the profile with the fiber should be located at $h = h_m$ and $h = 0$, respectively (Figure 3), one can also write the so-called transversality conditions[20]

$$\frac{\partial}{\partial\phi_h}F(h,\phi,\phi_h)\Big|_{h=0} = 0 \qquad \left[F(h,\phi,\phi_h) - \phi_h\frac{\partial}{\partial\phi_h}F(h,\phi,\phi_h)\right]\Big|_{h=h_m} = 0 \quad (A.14)$$

which can be rewritten as

$$\frac{1}{\sqrt{1+(R+h)^2\phi_h^2}}\Big|_{h=h_m} = 0 \quad (A.15)$$

$$\frac{\phi_h}{\sqrt{1+R^2\phi_h^2}}\Big|_{h=0} = \frac{b}{R} \quad (A.16)$$

The first condition, A.15, or, equivalently, $\phi_h|_{h=h_m} = \infty$ ($h_\phi|_{\phi=0} = 0$), reflects the fact that the tangent to the drop profile at its apex should be normal to the polar radius at the apex. The second condition together with eq 21 provides the value of microcontact angle θ_0

$$\cos\theta_0 = -b \quad (A.17)$$

Appendix B. Solution of the Equation for the Drop Profile

Let us introduce the function

$$\Psi(h) = \frac{(R+h)\phi_h}{\sqrt{1+(R+h)^2\phi_h^2}} \quad (B.1)$$

which is related to the profile curvature $\kappa(h)$ through the

equation

$$\frac{d\Psi(h)}{dh} + \frac{\Psi(h)}{R+h} = \kappa(h) \tag{B.2}$$

Then, eq 19 becomes a first order differential equation

$$\frac{d\Psi(h)}{dh} + \frac{\Psi(h)}{R+h} - a_1\Phi^l_{LS}(h) = \lambda_c \tag{B.3}$$

which has the general solution

$$\Psi(h) = \frac{\lambda_c}{2}(R+h) - a\frac{D(h)}{R+h} + \frac{C}{R+h} \tag{B.4}$$

where C is a constant of integration

$$a = \frac{1}{4K_1}\frac{\epsilon_{LS}\rho_S}{\epsilon_{LL}\rho_L}\left(\frac{\sigma_{LS}}{\sigma_{LL}}\right)^4 \tag{B.5}$$

$$K_1 = \frac{17}{16} - \frac{3}{8}\Delta^2 + \frac{1}{2}\Delta^3 - \frac{3}{16}\Delta^4 - \frac{\rho_{LV}}{\sigma_{LL}\rho_L}(1-\Delta^3) \tag{B.6}$$

and

$$D(h) = -\frac{a_1}{a}\int \Phi^l_{LS}(h)(R+h)\,dh \tag{B.7}$$

Using eq 6 for the potential $\Phi^l_{LS}(h)$, eq 28 becomes

$$D(h) = \frac{k\sigma_{LS}}{(2-\nu)\left(1+\frac{h}{\sigma_{LS}}\right)^{\nu-2}} + \frac{kR_f}{(1-\nu)\left(1+\frac{h}{\sigma_{LS}}\right)^{\nu-1}} \tag{B.8}$$

Combining the boundary condition A.16 with eqs B.1 and A.17 leads to $\Psi(0) = -\cos\theta_0$ which provides the following expression for C

$$C = -R\cos\theta_0 - \frac{\lambda_c}{2}R^2 + aD(0) \tag{B.9}$$

Hence, function $\Psi(h)$ becomes

$$\Psi(h) = \frac{1}{R+h}\left\{-R\cos\theta_0 + \frac{\lambda_c}{2}h(h+2R) - a[D(h) - D(0)]\right\} \tag{B.10}$$

Equation B.1 can be rewritten as

$$\phi_h = \frac{\Psi(h)}{(R+h)\sqrt{1-\Psi^2(h)}} \tag{B.11}$$

which has the obvious solution

$$\phi(h) - \phi_0 = \int_0^h \frac{\Psi(h)}{(R+h)\sqrt{1-\Psi^2(h)}}\,dh \tag{B.12}$$

where the constant of integration (ϕ_0) can be determined from the condition for the drop apex to be located on the polar axis of the coordinate system [$\phi(h_m) = 0$]. One thus obtains the expression

$$\phi_0 = -\int_0^{h_m} \frac{\Psi(h)}{(R+h)\sqrt{1-\Psi^2(h)}}\,dh \tag{B.13}$$

After the determination of ϕ_0 and C, eq B.12 still contains two unknown parameters, λ_c and h_m. A connection between them is provided by the boundary condition eq A.15, which together with eq B.11 leads to $\Psi(h_m) = \pm 1$. The correct sign of $\Psi(h_m)$ can be selected by observing that near the drop apex the derivative ϕ_h must be negative because $\phi(h)$ should increase with decreasing h. According to eq B.1 the functions $\Psi(h)$ and $\phi(h)$ have the same sign and therefore $\Psi(h_m) = -1$. The latter condition provides the following expression for λ_c

$$\lambda_c = -\frac{2}{h_m(h_m+2R)} \times \{(1-\cos\theta_0)R + h_m - a[D(h_m) - D(0)]\} \tag{B.14}$$

References and Notes

(1) Carroll, B. J. *Langmuir* **1986**, *2*, 248.
(2) Adam, N. K. *J. Soc. Dyers Colour.* **1937**, *53*, 122.
(3) Carroll, B. J. *J. Colloid Interface Sci.* **1976**, *57*, 488.
(4) Carroll, B. J. *J. Colloid Interface Sci.* **1984**, *97*, 195.
(5) Brochard, F. *J. Chem. Phys.* **1986**, *84*, 637.
(6) McHale, G.; Käb, N. A.; Newton, M. I.; Rowan, S. M. *J. Colloid Interface Sci.* **1997**, *186*, 453.
(7) Neimark, A. V. *J. Adhes. Sci. Technol.* **1999**, *13*, 1137.
(8) Berim, G. O.; Ruckenstein, E. *J. Colloid Interface Sci.* **2005**, *286*, 681.
(9) Bauer, C.; Dietrich, S. *Phys. Rev. E.* **2000**, *62*, 2428.
(10) McHale, G.; Newton, M. I.; Carroll, B. J. *Oil Gas Sci. Technol.* **2000**, *56*, 47.
(11) McHale, G.; Newton, M. I. *Colloids Surf.* **2002**, *206*, 79.
(12) Berim, G. O.; Ruckenstein, E. *J. Phys. Chem. B* **2004**, *108*, 19330.
(13) Berim, G. O.; Ruckenstein, E. *J. Phys. Chem. B* **2004**, *108*, 19339.
(14) (a) Derjaguin, B. V. *Acta Phys. Chem.* **1940**, *12*, 181. (b) Derjaguin, B. V. *J. Colloid Interface Sci.* **1974**, *49*, 249.
(15) Miller, C. A.; Ruckenstein, E. *J. Colloid Interface Sci.* **1974**, *48*, 368.
(16) Ruckenstein, E.; Lee, P. S. *Surf. Sci.* **1975**, *52*, 298.
(17) Lee, S. H.; Rossky, P. J. *J. Phys. Chem.* **1994**, *100*, 3334.
(18) *Handbook of Mathematic Functions with Formulas, Graphs, and Mathematical Tables*; Abramovitz, M., Stegun, I., Eds.; Dover: New York, 1972.
(19) Sharma, A. *Langmuir* **1993**, *9*, 3580.
(20) Elsgolc, L. E. In *Calculus of Variations*; Pergamon Press: Addison-Wesley: New York, 1962.